PLOS | ONE

RESEARCH ARTICLE

Tumor T_1 Relaxation Time for Assessing Response to Bevacizumab Anti-Angiogenic Therapy in a Mouse Ovarian Cancer Model

Murali K. Ravoori[1☯], Masato Nishimura[2☯], Sheela P. Singh[1], Chunhua Lu[3], Lin Han[1], Brian P. Hobbs[4], Sunila Pradeep[3], Hyun J. Choi[3], James A. Bankson[5], Anil K. Sood[3,6,7☯], Vikas Kundra[1,8☯*]

1 Department of Cancer Systems Imaging, U.T.- M.D. Anderson Cancer Center, Houston, Texas, United States of America, **2** Department of Obstetrics and Gynecology, The University of Tokushima Graduate School, Tokushima, Japan, **3** Department of Gynecologic Oncology, U.T.- M.D. Anderson Cancer Center, Houston, Texas, United States of America, **4** Department of Biostatistics, U.T.- M.D. Anderson Cancer Center, Houston, Texas, United States of America, **5** Department of Imaging Physics, U.T.- M.D. Anderson Cancer Center, Houston, Texas, United States of America, **6** Department of Cancer Biology, U.T.- M.D. Anderson Cancer Center, Houston, Texas, United States of America, **7** Center for RNA Interference and Non-Coding RNA, U.T.- M.D. Anderson Cancer Center, Houston, Texas, United States of America, **8** Department of Radiology, U.T.- M.D. Anderson Cancer Center, Houston, Texas, United States of America

☯ These authors contributed equally to this work.
* vkundra@mdanderson.org

OPEN ACCESS

Citation: Ravoori MK, Nishimura M, Singh SP, Lu C, Han L, Hobbs BP, et al. (2015) Tumor T_1 Relaxation Time for Assessing Response to Bevacizumab Anti-Angiogenic Therapy in a Mouse Ovarian Cancer Model. PLoS ONE 10(6): e0131095. doi:10.1371/journal.pone.0131095

Editor: Chryso Kanthou, University of Sheffield, UNITED KINGDOM

Received: July 18, 2014

Accepted: May 28, 2015

Published: June 22, 2015

Data Availability Statement: All relevant data are within the paper and its Supporting Information files.

Funding: This work was supported by grants from the NIH (CA109298, CA159042, P50CA083639, U54CA151668, CA016672). The funders had no role in study design, data collection and analysis, decision to publish, or preparation of the manuscript.

Competing Interests: The authors have declared that no competing interests exist.

Abstract

Purpose

To assess whether T_1 relaxation time of tumors may be used to assess response to bevacizumab anti-angiogenic therapy. Procedures: 12 female nude mice bearing subcutaneous SKOV3ip1-LC ovarian tumors were administered bevacizumab (6.25ug/g, n=6) or PBS (control, n=6) therapy twice a week for two weeks. T_1 maps of tumors were generated before, two days, and 2 weeks after initiating therapy. Tumor weight was assessed by MR and at necropsy. Histology for microvessel density, proliferation, and apoptosis was performed.

Results

Bevacizumab treatment resulted in tumor growth inhibition ($p<0.04$, n=6), confirming therapeutic efficacy. Tumor T_1 relaxation times increased in bevacizumab treated mice 2 days and 2 weeks after initiating therapy ($p<.05$, n=6). Microvessel density decreased 59% and cell proliferation (Ki67+) decreased 50% in the bevacizumab treatment group ($p<.001$, n=6), but not apoptosis.

Conclusions

Findings suggest that increased tumor T_1 relaxation time is associated with response to bevacizumab therapy in ovarian cancer model and might serve as an early indicator of response.

Introduction

Angiogenesis is the process of new blood vessel growth from pre-existing vessels and is crucial for cancer cell growth. Angiogenic vessels tend to be abnormal, for example, they have heterogeneous and disorganized structure [1] and increased permeability. The process is regulated by a balance of proangiogenic and antiangiogenic factors, which, upon the switch of tumor cells to an angiogenic phenotype, leads to tumor growth and progression. The rationale of anti-angiogenic therapy is based on the concept that normalization of tumor vasculature, pruning of abnormal vessels, and blockage of new angiogenesis causes tumor stabilization [2,3]. The vascular endothelial growth factor (VEGF) family of proteins and receptors play key roles in this process.

Bevacizumab (Genentech, Inc., South San Francisco, CA) is a humanized anti-VEGF monoclonal IgG1 antibody that inhibits the VEGF pathway. It was first approved by the U.S Food and Drug Administration (FDA) in 2004 for the treatment of advanced colorectal cancer in combination standard chemotherapy. Subsequently, it was approved for the treatment of advanced non-small cell lung cancer, kidney cancer and glioblastoma [4–12].

Ovarian cancer is the most lethal among gynecologic malignancies and therapies beyond surgery are not very effective. Therapies targeting the stroma, such as angiogenesis inhibitors, represent novel approaches. In ovarian cancer, prospective clinical trials have been conducted using Bevacizumab [13–16]. Among these, the largest single agent trial, Gynecologic Oncology Group (GOG) 170D trial, found a 21% response rate in patients with recurrent ovarian cancer; and, 40% of patients were progression free at 6-months [13]. Predicting response would aide patient selection for efficacy and avoid futile therapy and its complications. The mechanism of bevacizumab is to bind circulating VEGF, which inhibits its binding to its receptors on endothelial cells, thereby, altering their function and growth. The functional changes such as decreased capillary permeability and morphologic reduction in micro-vascular number should result in altered tissue characteristics, such as spin-lattice relaxation time constant (T_1). Magnetic resonance imaging (MRI) provides excellent imaging resolution and contrast without ionizing radiation. It is based on the measurement of the spatial distribution of hydrogen nuclei, as weighted by relaxation processes that are based on their local and molecular environment in a magnetic field. T_1 characterizes the rate of return of longitudinal signal to equilibrium. T_1-weighted images are commonly viewed clinically, but are usually not obtained quantitatively. In this work, we employ quantitative T_1 assessment. Tissues have characteristic relaxation time constants that can be altered physiologically or by disease [17–19]. Thus, therapy also has potential to alter T_1. Using T_1 for predicting response to angiogenic therapy is under investigation [20, 21]. Whether the T_1 relaxation times of tumors can be used to assess response to angiogenic therapy with bevacizumab is not known for ovarian cancer. We assessed whether the T_1-value of tumors could be used to assess response to bevacizumab anti-angiogenic therapy in a human ovarian cancer xenograft model.

Material and Methods

Cell culture

The ovarian cancer cell line SKOV3ip1-LC derived from ovarian adenocarcinoma was cultured in RPMI-1640 medium supplemented with 10% FBS and antibiotics (50μg/mL gentamicin sulfate, Cellglo, Medlatech, Inc. Manassas VA) at 37°C in a 5% carbon dioxide atmosphere.

Animals

Female athymic nude mice (NCr-nu) were purchased from the National Cancer Institute, Frederick Cancer Research and Development Center (Frederick, MD) and maintained in specific pathogen-free conditions. The animals were cared for according to guidelines set forth by the American Association for Accreditation of Laboratory Animal Care and the US Public Health Service Policy on Human Care and Use of Laboratory Animals. All mouse studies were approved and supervised by the University of Texas-M.D. Anderson Institutional Animal Care and Use Committee (protocol 01-12-01331). The protocol included sacrifice of animals that are moribund or that have excess tumor burden.

$1x10^6$ cells were subcutaneously injected in 12 female nude mice at the flank near the spine to mitigate motion on subsequent MR. Two weeks later, MR imaging was performed to assess tumor size and to obtain T_1 maps pre-therapy. Subsequently, the animals were randomly divided into two groups of six each. The treatment group received intraperitoneal injection of bevacizumab (6.25ug/g in 200uL of phosphate buffered saline, PBS) twice a week for two weeks. The control group received intraperitoneal injections of PBS on the same schedule. MR imaging was also performed two days and two weeks after initiating therapy. Two weeks after the start of therapy, the mice were sacrificed, tumor weight was recorded, and tissue divided for formalin fixation or were frozen in optimal cutting temperature (OCT) media.

Magnetic Resonance Imaging

MR imaging was performed pre-therapy then two days and two weeks after initial treatment. All MR studies were performed using a 4.7T scanner (Bruker Biospec, 47/40 USR, Bruker Biospin, Billerica, MA) with a 60-mm gradient insert and a volume resonator with a 35 mm inner diameter. Animals were anesthetized with 2% isofluorane and placed head first and prone on a positioning sled. Orthogonal 3-plane scout scans were initially acquired to confirm animal positioning. Animal placement and tumor location were confirmed using axial and coronal T2-weighted images (repetition time = 2750 ms, effective echo time (TE) = 50 ms, echo train = 8; field of view (FOV) = 4cm x 3cm, slice thickness = 1 mm, image matrix = 128 x128, number of signal averages = 2). Quantitative T_1 assessment was performed. A fast spin-echo saturation-recovery sequence (TR = 110–10,000 ms [110ms, 200ms, 400ms, 600ms, 1,000ms, 2,000ms, 4,000ms, 6,000ms, 10,000ms]; TE = 50 ms; echo train = 8; field of view (FOV) = 4cm x 3cm; Image matrix = 128 x128; number of signal averages = 1) was used to measure the T_1 of tumor tissue using regions of interest (ROI's) encompassing the entire tumor. T_2-weighted images were used to aide identification of tumor margins. Paravision version 4 was used to calculate the T_1 relaxation values by exponentially fitting of signal as a function of TR. Manually drawn regions of interest on each T2-weighted image containing tumor were used to derive tumor weight as described previously [22]. Briefly, using Image J software (National Institutes of Health, USA), in each image containing a tumor, the periphery of the mass was traced and the area of the drawn region was calculated. The areas were then multiplied by the slice thickness plus skip to obtain the volume of tumor in each slice and these volumes added. Assuming a tissue density of 1 g/ml, to derive weight, volume in mm^3 was multiplied by .001 g of tissue/mm^3.

Immunohistochemistry

Immunohistochemical staining for Ki67 and CD31 was performed. For Ki67 staining, formalin-fixed paraffin-embedded tissue samples were cut into 5-μm sections. After deparaffinization, antigen retrieval was performed by heating the slide in a steam cooker for 10 minutes in 0.2M Tris buffer, pH 9.0. CD31 was stained [23] using frozen slides. Endogenous peroxide was blocked with 3% H_2O_2 in methanol for 12 minutes. After protein block with normal horse and

goat serum, slides were incubated with primary antibody to Ki67 (Thermo scientific, Fremont, CA) or CD31 (PECAM-1, 1:800 rat IgG, Pharmingen, San Diego, CA) in blocking solution overnight at 4°C. After washing with PBS three times, the HRP-conjugated anti-mouse secondary antibody (DAKO, Carpinteria, CA) in blocking solution was added for one hour at room temperature. Slides were stained with DAB substrate (Phoenix Biotechnologies, Huntsville, AL) and counterstained with Gils No. 3 hematoxylin (Sigma-Aldrich, St. Louis, MO). To quantify micro-vessel density (MVD), the micro-vessels within five randomly selected 0.159-mm^2 fields at 100X were counted. A single micro-vessel was defined as a discrete cluster or at least three cells stained positive for CD31. The presence of a lumen was required for scoring as a micro-vessel. The Ki67 labelling index was determined by counting at least 1,000 tumor cells and the index was calculated as a percentage. TUNEL assay was performed as described [23].

Statistical analysis

For comparing groups, 2 tailed t-tests were performed using spreadsheet software (Microsoft Office Excel 2003, Microsoft, Seattle, WA). Least squares linear regression was used to evaluate the extent of linear dependence between MR derived tumor weight and excised tumor weight. Repeated measures ANOVA was used to compare the extent of relative change in T_1 relaxation time (pre-treatment to follow-up scans at 48 hours and 2 weeks) between bevacizumab and control mice. Random intercepts were used to adjust the inference for inter-mouse heterogeneity by accounting for interdependence among the three repeated intra-mouse scans. Two-sided Wald tests using the robust estimation method described by Koller and Stahel [24] were applied to fixed effects characterizing the mean difference between Bevacizumab and control in the extent of relative change in T_1 relaxation time at each of the two follow-up scans. This test does not assume a Gaussian distribution enabling evaluation of data even with non-normal, skewed distribution. Bonferroni correction was used to control the familywise type I error rate at the 0.05 significance level among the two tests for differences in the extent of relative change at each follow-up scan, inducing a significance threshold of 0.025 for each test. ANOVA was implemented using the statistical software R (R Development Core Team, http://www.r-project.org) version 3.0 using the *robustlmm* package.

Results

Tumor size

We evaluated the effect of bevacizumab on tumor growth. Bevacizumab treatment inhibited tumor growth compared to the control as seen by MR imaging (Fig 1). Before therapy, there was no statistically significant difference in tumor weight between the two groups as measured on the MR images. Two days and two weeks post-treatment, mice treated with bevacizumab had significantly smaller tumors than control mice ($p< 0.04$, $n = 6$) by both in vivo MR measurement and ex vivo at necropsy (Fig 2). No difference was seen in tumor weights in the treatment groups pre-therapy versus 2 days or 2 weeks post initiation of bevacizumab therapy. Tumor weights derived from in vivo MR imaging correlated highly with the weights of excised tumors ($r^2 = 0.99$, $p<0.001$, $n = 12$, Fig 3).

T_1 values

The T_1 relaxation time was significantly increased in the bevacizumab treated group compared to controls, both two days (2302±567, mean ± standard deviation, vs 1729±209) and two weeks (2146±276 vs 1847±112) after initiation of therapy ($p< 0.05$, $n = 6$, Fig 4). There was variation in the T_1 values (S1 Fig); therefore, to adjust for potential skewness in these comparisons, two-

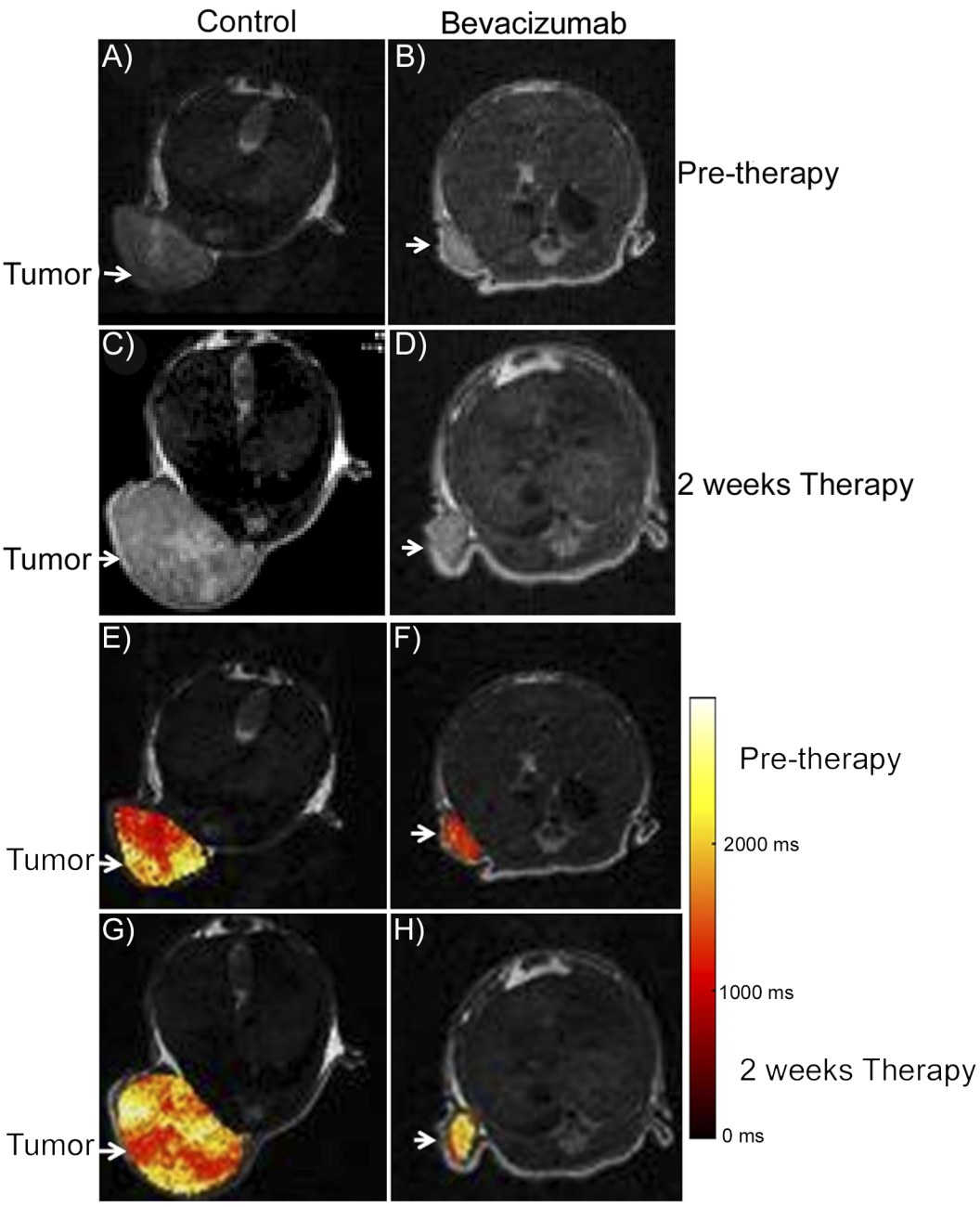

Fig 1. Axial T2-weighted MR imaging of mice with tumors. Representative axial MR images of mice pre-therapy (A, B) or two weeks after initiation of therapy (C, D) with vehicle (A, C) or bevacizumab (B, D). Axial T1 maps of the same tumors (E, F, G, H). Representative axial MR images of mice pre-therapy (E, F) or two weeks after initiation of therapy (G, H) with vehicle (E, G) or bevacizumab (F, H).

doi:10.1371/journal.pone.0131095.g001

sided Wald tests using the robust estimation method described by Koller and Stahel [24] were applied. Significant differences in the extent of T_1 relaxation time modification were evident between bevacizumab and control cohorts at each follow-up scan after adjusting for multiplicity. Statistically, robust inference estimates that the extent of relative change in T_1 relaxation time was 16.1% ($p \leq 0.011$) larger on average for bevacizumab treated mice when compared to control mice after 48 hours. The result maintained statistical significance after 2 weeks, where

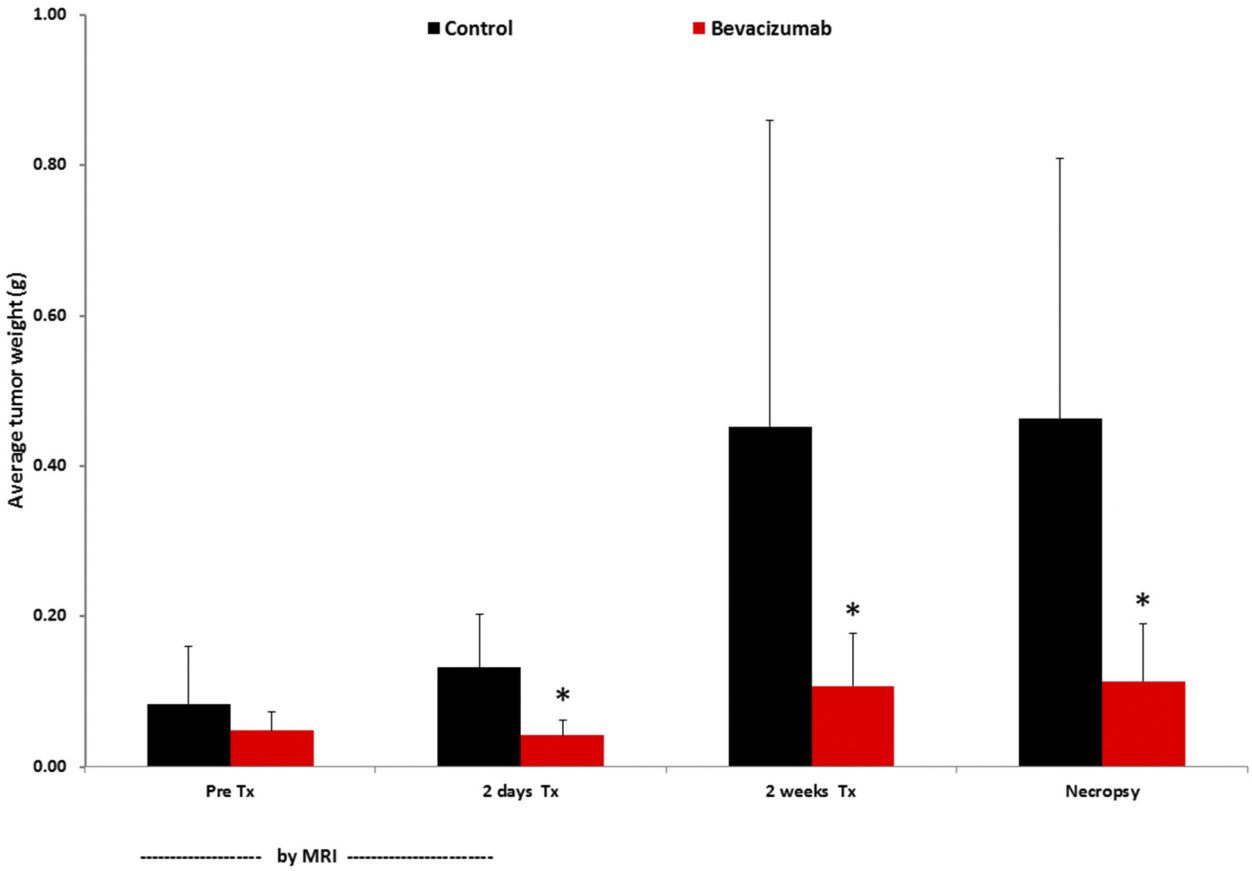

Fig 2. Tumor growth. Tumor weight derived from MR images before and two weeks after initiation of therapy, and, by necropsy two weeks after initiation of therapy. *, p<.05. Error bars represent standard deviation.

doi:10.1371/journal.pone.0131095.g002

T_1 relaxation time was increased by 14.5% (p-value$\leq$0.021) on average for bevacizumab treated mice. Prior to treatment, T_1 relaxation time was 1877±60 for tumors from mice that subsequently were treated with bevacizumab. In comparison, the T_1 value did not change from pre-therapy levels (1875±57) in the control group despite increase in tumor size.

Histology

Mean vessel density, proliferation, and apoptosis were evaluated as histologic biomarkers of the effects of bevacizumab at two weeks post initiation of therapy. CD31 staining was used to mark vessels. The average mean vessel density was decreased by 59% in the bevacizumab treatment group compared to the control group ($p<0.001$, n = 6, Fig 5A). Ki67 was used as a marker of cellular proliferation. Ki67 labelling index was decreased by 50% in the bevacizumab treatment group ($p<0.0001$, Fig 5B) compared to the control group. On the other hand, apoptotic index, evaluated using TUNEL staining, was not different between the two groups (Fig 5C).

Discussion

Anti-angiogenic therapy with bevacizumab results in treatment response in a subset of patients with ovarian cancer. Markers of response are needed to parse those patients who may benefit from therapy versus futile therapy for patients who would be at risk of complications without therapeutic benefit. Anti-angiogenic therapy alters the function and morphology of blood

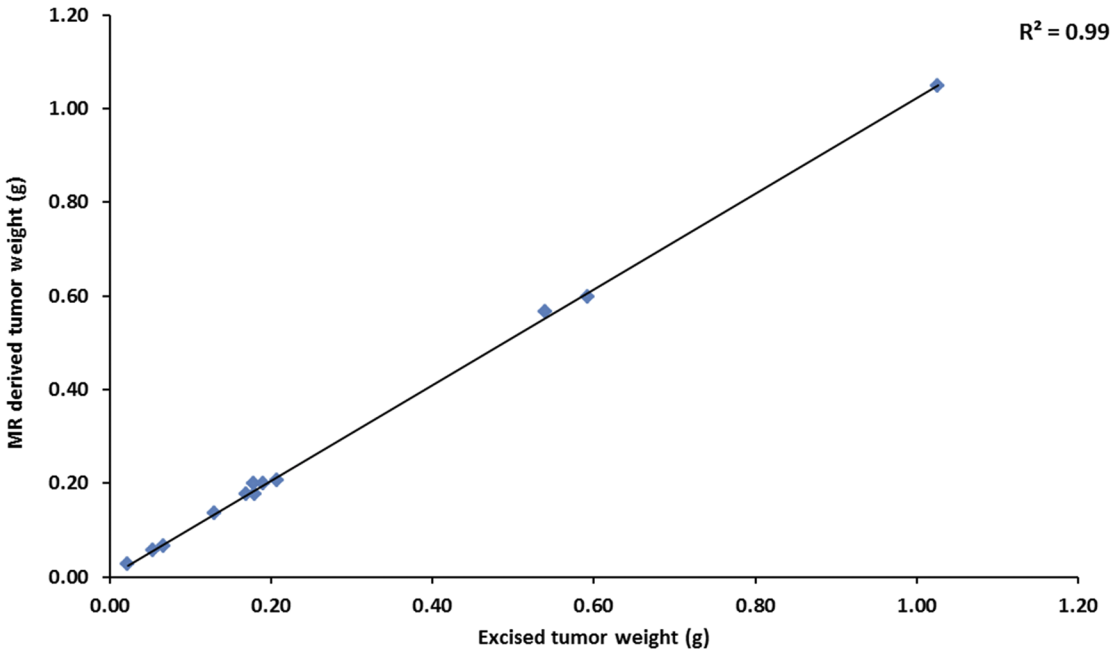

Fig 3. Correlation of tumor weight by MR and ex vivo.

doi:10.1371/journal.pone.0131095.g003

vessels within tumor tissue. Our data suggest that the increased T_1 relaxation time of tumor tissue provides an early indication of response to bevacizumab anti-angiogenic therapy. This is the first report that we are aware that evaluates T_1 relaxation time in the context of ovarian tumor anti-angiogenic therapy.

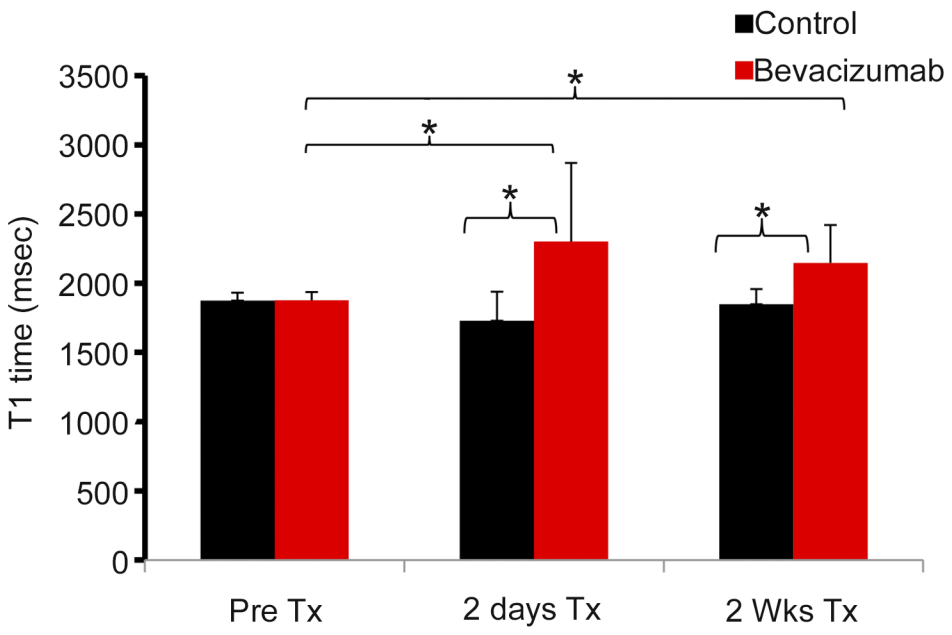

Fig 4. T1 values pre and post therapy. T1 values of tumors pre, 48 hour, and two weeks post therapy. *, p<.05. Error bars represent standard deviation.

doi:10.1371/journal.pone.0131095.g004

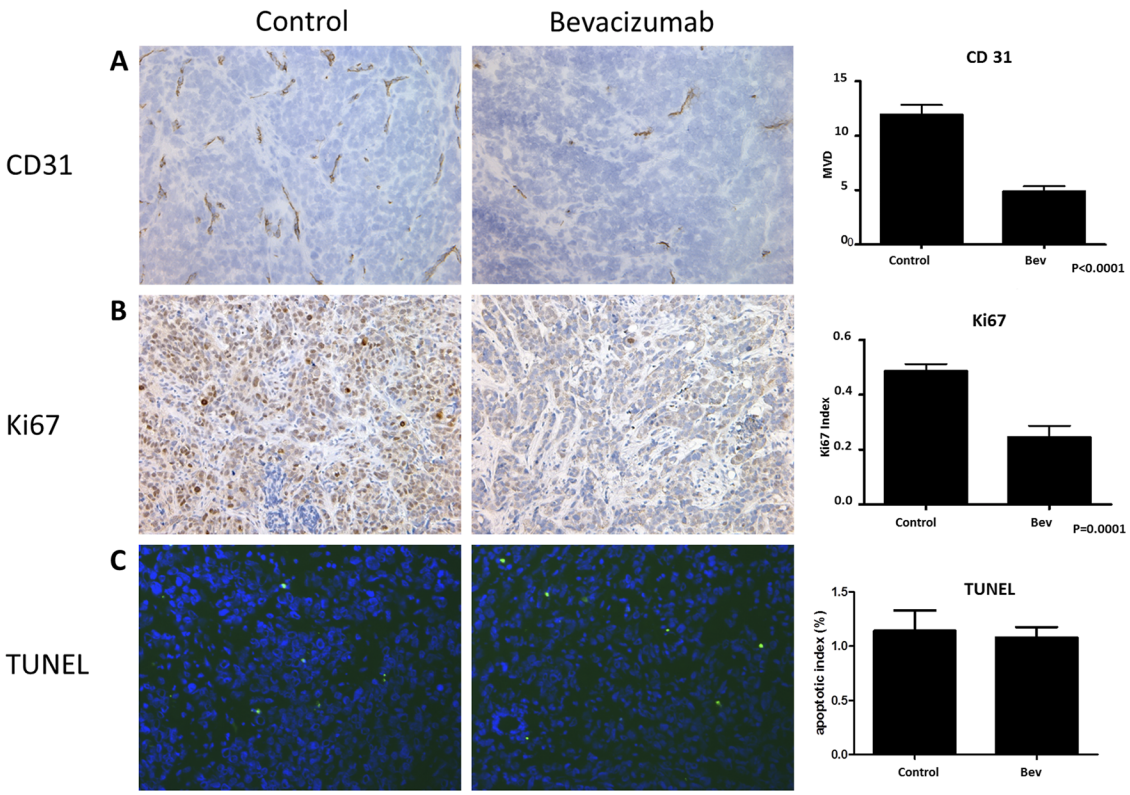

Fig 5. Histologic analysis of mean vessel density, proliferation, and apoptosis 2 weeks post-initiation of therapy. A) Immunohistochemical staining for CD31 (left) and microvessel density (right). B) Immunohistochemical staining for Ki67 (left) and Ki67 labelling index (right). C) TUNEL staining (left) and apoptotic index (right). Error bars represent standard deviation.

doi:10.1371/journal.pone.0131095.g005

Histologic examination of tumor tissue showed decrease in microvessel density and proliferation in the bevacizumab treatment group. Tumor growth was also inhibited. These findings are consistent with altered tumor architecture and functional change in tumor growth. In contrast, the rate of apoptosis was not changed. These result are consistent with the data of Rapisarda et al. [25] who reported that microvessel density was decreased and hypoxia inducible factor-1 (HIF-1) dependent gene expression was increased after treatment of U251 (glioblastoma) tumors with bevacizumab, but apoptosis was not induced.

Abnormal blood and lymphatic vessels, including poor permeability selectivity due to high vascular permeability result in increased tumor interstitial fluid pressure (IFP) [26]. Anti-angiogenic treatment results in a decrease in microvessel density, vascular permeability and interstitial fluid pressure (IFP) [27]. In patients with rectal cancer, overall mean IFP decreased 15.0 mm Hg after treatment with bevacizumab [28]. This may affect fluid sensitive parameter T_1 [26] since IFP is related to fluid in the extracellular-extravascular space.

Anti-angiogenesis therapy has been evaluated in a number of clinical trials using dynamic contrast enhanced MR imaging and these have commonly demonstrated decrease in the forward directional transfer coefficient, k^{trans}, and initial area under the curve, IAUC, and in some studies, the unidirectional influx constant K_i, but few have been linked to increased progression free or overall survival [29]. For bevacizumab, decreased k^{trans} has been noted [30] and although this is a complex parameter, the finding suggests decreased permeability. This appears to be a common finding and has also been suggested in several tumor models [31–33].

Thus, bevacizumab therapy has effects on several vascular parameters that effect tumor structure and behavior. This can affect the imaging characteristics of tumors. For example, in patients receiving cytotoxic therapy plus bevacizumab for 2–3 months, tumor morphology change by CT, including homogeneous low attenuation and sharp borders of colorectal liver metastases corresponded with decreased residual tumor [34]. MR has greater soft tissue contrast than CT. Most tumors involving the liver have a longer T_1 than normal liver, thus, most metastases appear to be of lower signal on T_1-weighted MR. Standard T_1 weighted imaging is qualitative and can be influenced by a number of parameters such as hardware related effects, coil loading and sequence parameters, moreover, perception of change is dependent on windowing and leveling of images; in comparison, T_1 relaxometry gives more quantitative results and can result in improved sensitivity to tissue biochemical and structural changes with pathology [35]. T_1 mapping evaluates tissue T_1 effects, removing contamination such as proton density, T_2, and coil sensitivity that influence standard T_1 weighted imaging [35].

The difference in T_1 relaxivity of tissue enables differentiation of different tissue types. Disease of a tissue can alter T_1 relaxation time, for example, it is increased in patients with cirrhosis compared to normal liver or chronic hepatitis [36], suggesting that the fibrotic architectural change in the liver lengthens this value. T_1 relaxation time has been used in patients to derive water content in the brain [19] and increased T_1 relaxation time was found to correspond with increased edema in the myocardium [37], i.e. increased fluid in the extravascular-extracellular space. Theoretically, by decreasing interstitial pressure, the amount of fluid in the extravascular-extracellular space should decrease with bevacizumab therapy resulting in decreased T_1 relaxation time. However, bevacizumab has multiple other effects such as vessel pruning and normalization, and, as we noted, decreased tumor cell proliferation. We noted an increase in T_1 relaxation time at two days and two weeks post-therapy, suggesting that other effects of bevacizumab on tissue parameters such as on blood flow, cellularity, architecture, and lymphatic drainage may have contributed to the increased T_1 relaxation time that overwhelmed the theoretical decrease in T_1 relaxation time expected from inhibiting vascular permeability alone.

T_1 relaxation time has been evaluated in prior mouse studies in the setting of chemotherapy. McSheehy et al. evaluated several chemotherapeutics that cause shrinkage of tumors and found decrease in T_1 relaxation time with response, including an angiogenesis inhibitor PTK/ZK on murine B16/BL6 melanoma tumors [38]. Weidensteiner et al. from the same group also found decrease in T_1 relaxation time in response to an mTOR inhibitor in RIF-1 fibrosarcoma tumors and decrease in Ki67, but not mean vessel density [39]. Older studies have noted increase or decrease of T_1 relaxation time with treatment [40–43]. Differences may be due to the therapeutic, animal model, and different methods of calculating T_1 relaxation time. In addition, increased fractional tumor water content results in longer T_1, and although correlations are not very strong, necrosis can result in shorter T_1 thought to be due to release of complexed paramagnetic ions/proteins with development of necrosis [43,44]. We noted no difference in tumor size or T_1 relaxation times between treated and untreated groups pre-therapy, and without therapy, the T_1 relaxation time did not change despite enlarging tumors. With bevacizumab therapy, tumor growth was inhibited; and, in these tumors, as early as two days post therapy, T_1 relaxation time increased. At two weeks, growth was still inhibited compared to the no therapy group and T_1 relaxation time was still increased. Mechanistically, the increased T_1 relaxation time corresponds with decreased proliferation and decreased mean vessel density as seen in Fig 5, suggesting that more extra-cellular extra-vascular space became available for fluid. A limitation of this paper is that extra-cellular extra-vascular space was not directly measured, however, prior reports also suggest that increased T_1 suggests increased extracellular volume [45]. A potential limitation of this paper is use of subcutaneous tumors. Although orthotopic models are commonly used, so are subcutaneous models [46–49]. A problem for intra-

abdominal imaging of the mouse by MR is that it is prone to motion artifact due to breathing. Due to the relatively long acquisition times needed for T_1 mapping, we wanted to limit the potential of motion artifacts interfering with the T_1 calculation. Therefore, we used a subcutaneous model where the tumor could be placed near the spine to mitigate motion. Methods for T_1 mapping in clinically feasible times are being approached [50].

In the future, this affords the potential for multiparametric imaging including dynamic contrast imaging to evaluate vascular permeability, diffusion weighted imaging to assess molecular motion, and T_1 mapping to evaluate T_1-relaxivity to predict response to anti-angiogenic therapy. Methods for simultaneous quantification of relative proton density, T_1, and T_2 in time frames approachable for clinical use [50] suggest the potential of expanded multiparametric quantitative MR, including T_1 relaxation time measurements, to be applied to patients with ovarian cancer.

Conclusion

Findings suggest that increased tumor T_1 relaxation time is associated with response to bevacizumab therapy in ovarian cancer model and might serve as an early indicator of response.

Supporting Information

S1 Fig. Difference in T1-map value day 2 or week 2 vs pre-therapy for individual tumors in treatment groups from Fig 4.
(TIF)

Author Contributions

Conceived and designed the experiments: VK JAB. Performed the experiments: MKR MN SPS CL LH SP HJC JAB AKS VK. Analyzed the data: MKR MN SPS CL LH SP HJC BPH JAB AKS VK. Contributed reagents/materials/analysis tools: VK AKS JAB BPH. Wrote the paper: MKR MN SPS CL LH SP HJC BPH JAB AKS VK.

References

1. Helmlinger G, Yuan F, Dellian M, Jain RK (1997) Interstitial pH and pO2 gradients in solid tumors in vivo: high-resolution measurements reveal a lack of correlation. Nat Med 3: 177–182. PMID: 9018236
2. Ferrara N (2005) VEGF as a therapeutic target in cancer. Oncology 69 Suppl 3: 11–16. PMID: 16301831
3. Jain RK (2005) Antiangiogenic therapy for cancer: current and emerging concepts. Oncology (Williston Park) 19: 7–16.
4. Hurwitz H, Fehrenbacher L, Novotny W, Cartwright T, Hainsworth J, Heim W et al. (2004) Bevacizumab plus irinotecan, fluorouracil, and leucovorin for metastatic colorectal cancer. N Engl J Med 350: 2335–2342. PMID: 15175435
5. Kabbinavar F, Hurwitz HI, Fehrenbacher L, Meropol NJ, Novotny WF, Lieberman G et al. (2003) Phase II, randomized trial comparing bevacizumab plus fluorouracil (FU)/leucovorin (LV) with FU/LV alone in patients with metastatic colorectal cancer. J Clin Oncol 21: 60–65. PMID: 12506171
6. Saltz LB, Clarke S, Diaz-Rubio E, Scheithauer W, Figer A, Wong R et al. (2008) Bevacizumab in combination with oxaliplatin-based chemotherapy as first-line therapy in metastatic colorectal cancer: a randomized phase III study. J Clin Oncol 26: 2013–2019. doi: 10.1200/JCO.2007.14.9930 PMID: 18421054
7. Giantonio BJ, Catalano PJ, Meropol NJ, O'Dwyer PJ, Mitchell EP, Alberts SR et al. (2007) Bevacizumab in combination with oxaliplatin, fluorouracil, and leucovorin (FOLFOX4) for previously treated metastatic colorectal cancer: results from the Eastern Cooperative Oncology Group Study E3200. J Clin Oncol 25: 1539–1544. PMID: 17442997
8. Reck M, von Pawel J, Zatloukal P, Ramlau R, Gorbounova V, Hirsh V et al. (2009) Phase III trial of cisplatin plus gemcitabine with either placebo or bevacizumab as first-line therapy for nonsquamous non-

small-cell lung cancer: AVAil. J Clin Oncol 27: 1227–1234. doi: 10.1200/JCO.2007.14.5466 PMID: 19188680

9. Sandler A, Gray R, Perry MC, Brahmer J, Schiller JH, Dowlati A et al. (2006) Paclitaxel-carboplatin alone or with bevacizumab for non-small-cell lung cancer. N Engl J Med 355: 2542–2550. PMID: 17167137
10. Miller K, Wang M, Gralow J, Dickler M, Cobleigh M, Perez EA et al. (2007) Paclitaxel plus bevacizumab versus paclitaxel alone for metastatic breast cancer. N Engl J Med 357: 2666–2676. PMID: 18160686
11. Miles DW, Chan A, Dirix LY, Cortes J, Pivot X, Tomczak P et al. (2010) Phase III study of bevacizumab plus docetaxel compared with placebo plus docetaxel for the first-line treatment of human epidermal growth factor receptor 2-negative metastatic breast cancer. J Clin Oncol 28: 3239–3247. doi: 10.1200/JCO.2008.21.6457 PMID: 20498403
12. Escudier B, Pluzanska A, Koralewski P, Ravaud A, Bracarda S, Szczylik C et al. (2007) Bevacizumab plus interferon alfa-2a for treatment of metastatic renal cell carcinoma: a randomised, double-blind phase III trial. Lancet 370: 2103–2111. PMID: 18156031
13. Burger RA, Sill MW, Monk BJ, Greer BE, Sorosky JI (2007) Phase II trial of bevacizumab in persistent or recurrent epithelial ovarian cancer or primary peritoneal cancer: a Gynecologic Oncology Group Study. J Clin Oncol 25: 5165–5171. PMID: 18024863
14. Cannistra SA, Matulonis UA, Penson RT, Hambleton J, Dupont J, Mackey H et al. (2007) Phase II study of bevacizumab in patients with platinum-resistant ovarian cancer or peritoneal serous cancer. J Clin Oncol 25: 5180–5186. PMID: 18024865
15. Garcia AA, Hirte H, Fleming G, Yang D, Tsao-Wei DD, Roman L et al. (2008) Phase II clinical trial of bevacizumab and low-dose metronomic oral cyclophosphamide in recurrent ovarian cancer: a trial of the California, Chicago, and Princess Margaret Hospital phase II consortia. J Clin Oncol 26: 76–82. doi: 10.1200/JCO.2007.12.1939 PMID: 18165643
16. Nimeiri HS, Oza AM, Morgan RJ, Friberg G, Kasza K, Faoro L et al. (2008) Efficacy and safety of bevacizumab plus erlotinib for patients with recurrent ovarian, primary peritoneal, and fallopian tube cancer: a trial of the Chicago, PMH, and California Phase II Consortia. Gynecol Oncol 110: 49–55. doi: 10.1016/j.ygyno.2008.02.009 PMID: 18423560
17. Damadian R (1971) Tumor detection by nuclear magnetic resonance. Science 171: 1151–1153. PMID: 5544870
18. de Graaf RA, Brown PB, McIntyre S, Nixon TW, Behar KL et al. (2006) High magnetic field water and metabolite proton T1 and T2 relaxation in rat brain in vivo. Magn Reson Med 56: 386–394. PMID: 16767752
19. Fatouros PP, Marmarou A (1999) Use of magnetic resonance imaging for in vivo measurements of water content in human brain: method and normal values. J Neurosurg 90: 109–115. PMID: 10413163
20. Jamin Y, Tucker ER, Poon E, Popov S, Vaughan L, Boult JK et al. (2013) Evaluation of clinically translatable MR imaging biomarkers of therapeutic response in the TH-MYCN transgenic mouse model of neuroblastoma. Radiology 266: 130–140. doi: 10.1148/radiol.12120128 PMID: 23169794
21. O'Connor JP, Carano RA, Clamp AR, Ross J, Ho CC, Jackson A et al. (2009) Quantifying antivascular effects of monoclonal antibodies to vascular endothelial growth factor: insights from imaging. Clin Cancer Res 15: 6674–6682. doi: 10.1158/1078-0432.CCR-09-0731 PMID: 19861458
22. Yang D, Han L, Kundra V (2005) Exogenous gene expression in tumors: noninvasive quantification with functional and anatomic imaging in a mouse model. Radiology 235: 950–958. PMID: 15914480
23. Kim TJ, Landen CN, Lin YG, Mangala LS, Lu C, Nick AM et al. (2009) Combined anti-angiogenic therapy against VEGF and integrin alphaVbeta3 in an orthotopic model of ovarian cancer. Cancer Biol Ther 8: 2263–2272. PMID: 19829059
24. Koller MSW (2011) Sharpening Wald-type inference in robust regression for small samples. Computational Statistics & Data Analysis 55: 2504–2515.
25. Rapisarda A, Hollingshead M, Uranchimeg B, Bonomi CA, Borgel SD, Carter JP et al. (2009) Increased antitumor activity of bevacizumab in combination with hypoxia inducible factor-1 inhibition. Mol Cancer Ther 8: 1867–1877. doi: 10.1158/1535-7163.MCT-09-0274 PMID: 19584228
26. Boucher Y, Jain RK (1992) Microvascular pressure is the principal driving force for interstitial hypertension in solid tumors: implications for vascular collapse. Cancer Res 52: 5110–5114. PMID: 1516068
27. Jain RK, Tong RT, Munn LL (2007) Effect of vascular normalization by antiangiogenic therapy on interstitial hypertension, peritumor edema, and lymphatic metastasis: insights from a mathematical model. Cancer Res 67: 2729–2735. PMID: 17363594
28. Willett CG, Boucher Y, di Tomaso E, Duda DG, Munn LL et al. (2004) Direct evidence that the VEGF-specific antibody bevacizumab has antivascular effects in human rectal cancer. Nat Med 10: 145–147. PMID: 14745444

29. Murukesh N, Dive C, Jayson GC (2010) Biomarkers of angiogenesis and their role in the development of VEGF inhibitors. Br J Cancer 102: 8–18. doi: 10.1038/sj.bjc.6605483 PMID: 20010945

30. Wedam SB, Low JA, Yang SX, Chow CK, Choyke P, Danforth D et al. (2006) Antiangiogenic and antitumor effects of bevacizumab in patients with inflammatory and locally advanced breast cancer. J Clin Oncol 24: 769–777. PMID: 16391297

31. Willett CG, Duda DG, di Tomaso E, Boucher Y, Ancukiewicz M, Sahani DV et al. (2009) Efficacy, safety, and biomarkers of neoadjuvant bevacizumab, radiation therapy, and fluorouracil in rectal cancer: a multidisciplinary phase II study. J Clin Oncol 27: 3020–3026. doi: 10.1200/JCO.2008.21.1771 PMID: 19470921

32. Siegel AB, Cohen EI, Ocean A, Lehrer D, Goldenberg A, Knox JJ et al. (2008) Phase II trial evaluating the clinical and biologic effects of bevacizumab in unresectable hepatocellular carcinoma. J Clin Oncol 26: 2992–2998. doi: 10.1200/JCO.2007.15.9947 PMID: 18565886

33. Varallyay CG, Muldoon LL, Gahramanov S, Wu YJ, Goodman JA, Li X et al. (2009) Dynamic MRI using iron oxide nanoparticles to assess early vascular effects of antiangiogenic versus corticosteroid treatment in a glioma model. J Cereb Blood Flow Metab 29: 853–860. doi: 10.1038/jcbfm.2008.162 PMID: 19142191

34. Chun YS, Vauthey JN, Boonsirikamchai P, Maru DM, Kopetz S, Palavecino M et al. (2009) Association of computed tomography morphologic criteria with pathologic response and survival in patients treated with bevacizumab for colorectal liver metastases. JAMA 302: 2338–2344. doi: 10.1001/jama.2009.1755 PMID: 19952320

35. Deoni SC, Williams SC, Jezzard P, Suckling J, Murphy DG, Jones DK (2008) Standardized structural magnetic resonance imaging in multicentre studies using quantitative T1 and T2 imaging at 1.5 T. Neuroimage 40: 662–671. doi: 10.1016/j.neuroimage.2007.11.052 PMID: 18221894

36. Katsube T, Okada M, Kumano S, Hori M, Imaoka I, Ishii K et al. (2011) Estimation of liver function using T1 mapping on Gd-EOB-DTPA-enhanced magnetic resonance imaging. Invest Radiol 46: 277–283. doi: 10.1097/RLI.0b013e318200f67d PMID: 21343827

37. Ferreira VM, Piechnik SK, Dall'armellina E, Karamitsos TD, Francis JM, Choudhury RP et al. (2012) Non-contrast T1-mapping detects acute myocardial edema with high diagnostic accuracy: a comparison to T2-weighted cardiovascular magnetic resonance. J Cardiovasc Magn Reson 14: 42. doi: 10.1186/1532-429X-14-42 PMID: 22720998

38. McSheehy PM, Weidensteiner C, Cannet C, Ferretti S, Laurent D, Ruetz S et al. (2010) Quantified tumor t1 is a generic early-response imaging biomarker for chemotherapy reflecting cell viability. Clin Cancer Res 16: 212–225. doi: 10.1158/1078-0432.CCR-09-0686 PMID: 20008843

39. Weidensteiner C, Allegrini PR, Sticker-Jantscheff M, Romanet V, Ferretti S, McSheey PM (2014) Tumour T1 changes in vivo are highly predictive of response to chemotherapy and reflect the number of viable tumour cells—a preclinical MR study in mice. BMC Cancer 14: 88. doi: 10.1186/1471-2407-14-88 PMID: 24528602

40. Le Moyec L, Pellen P, Merdrignac-Le Noan G, Le Lan J, Lancien G, Chenal C et al. (1988) Proton NMR relaxation times of experimental Lewis lung carcinoma after irradiation. Radiother Oncol 13: 1–8. PMID: 3187071

41. Chenevert TL, McKeever PE, Ross BD (1997) Monitoring early response of experimental brain tumors to therapy using diffusion magnetic resonance imaging. Clin Cancer Res 3: 1457–1466. PMID: 9815831

42. Duvvuri U, Poptani H, Feldman M, Nadal-Desbarats L, Gee MS, Lee WM et al. (2001) Quantitative T1rho magnetic resonance imaging of RIF-1 tumors in vivo: detection of early response to cyclophosphamide therapy. Cancer Res 61: 7747–7753. PMID: 11691788

43. Jakobsen I, Kaalhus O, Lyng H, Rofstad EK (1995) Detection of necrosis in human tumour xenografts by proton magnetic resonance imaging. Br J Cancer 71: 456–461. PMID: 7880724

44. Rofstad EK, Steinsland E, Kaalhus O, Chang YB, Hovik B, Lyng H (1994) Magnetic resonance imaging of human melanoma xenografts in vivo: proton spin-lattice and spin-spin relaxation times versus fractional tumour water content and fraction of necrotic tumour tissue. Int J Radiat Biol 65: 387–401. PMID: 7908318

45. Jakobsen I, Lyng H, Kaalhus O, Rofstad EK (1995) MRI of human tumor xenografts in vivo: proton relaxation times and extracellular tumor volume. Magn Reson Imaging 13: 693–700. PMID: 8569443

46. Cole CL, Rushton G, Jayson GC, Avizienyte E (2014) Ovarian cancer cell heparan sulfate 6-O-sulfotransferases regulate an angiogenic program induced by heparin-binding epidermal growth factor (EGF)-like growth factor/EGF receptor signaling. J Biol Chem 289: 10488–10501. doi: 10.1074/jbc.M113.534263 PMID: 24563483

47. Lutz AM, Bachawal SV, Drescher CW, Pysz MA, Willmann JK, Gambhir SS (2014) Ultrasound molecular imaging in a human CD276 expression-modulated murine ovarian cancer model. Clin Cancer Res 20: 1313–1322. doi: 10.1158/1078-0432.CCR-13-1642 PMID: 24389327

48. Utsumi F, Kajiyama H, Nakamura K, Tanaka H, Mizuno M, Ishikawa K et al. (2013) Effect of indirect nonequilibrium atmospheric pressure plasma on anti-proliferative activity against chronic chemo-resistant ovarian cancer cells in vitro and in vivo. PLoS One 8: e81576. doi: 10.1371/journal.pone.0081576 PMID: 24367486

49. Lawrenson K, Grun B, Lee N, Mhawech-Fauceglia P, Kan J, Swenson S et al. (2015) NPPB is a novel candidate biomarker expressed by cancer-associated fibroblasts in epithelial ovarian cancer. Int J Cancer 136: 1390–1401. doi: 10.1002/ijc.29092 PMID: 25047817

50. Ehses P, Seiberlich N, Ma D, Breuer FA, Jakob PM, Griswold MA et al. (2013) IR TrueFISP with a golden-ratio-based radial readout: fast quantification of T1, T2, and proton density. Magn Reson Med 69: 71–81. doi: 10.1002/mrm.24225 PMID: 22378141